SAN FRANCISCO ESTUARY & WATERSHED SCIENCE
Sponsored by the Delta Stewardship Council and UC Davis Institute of the Environment

RESEARCH

A Simple Approach to Modeling Light Attenuation in the Sacramento–San Joaquin Delta Using Commonly Available Data

Emily T. Richardson*[1], Keith Bouma–Gregson[1], Katy O'Donnell[1], Brian A. Bergamaschi[1]

ABSTRACT

The diffuse attenuation coefficient of photosynthetically active radiation (K_{dPAR}) is commonly used to predict light attenuation in aquatic productivity models, but obtaining measurements of PAR to compute K_{dPAR} is difficult. *In situ* calculations of K_{dPAR} require multiple measurements of PAR through the water column, and these measurements are infeasible for real-time recording. Instead, predictive models using surface-water measurements may be used. Traditional K_{dPAR} models are based on open-ocean habitats and rely on chlorophyll—as a proxy measurement for phytoplankton abundance—as the main predictive parameter. However, elevated suspended sediments and dissolved organic materials may also affect K_{dPAR} values of inland water bodies and estuaries. In this study, we leverage K_{dPAR} calculations derived from *in situ* light measurements collected along with surface-water-quality parameters across the Sacramento–San Joaquin River Delta in California, USA (the Delta). Sampling occurred between January of 2013 and May of 2014. We also explored regional and seasonal effects, but these did not clearly affect the model. Ultimately, the best-performing model included surface-level turbidity only ($R^2 = 0.91$). The simplicity of the model facilitates use of K_{dPAR} estimates for a variety of purposes throughout the Delta, including euphotic depth calculations, and as inputs to primary-productivity and habitat-suitability models. We demonstrate the model's usability with two open-sources data sets (one spatially dense, and one temporally dense), and estimate K_{dPAR}, euphotic depth, and primary productivity within the Delta. We provide calculations for each estimation, allowing users to easily adopt these models and apply them to their own data or with open-sourced data, which are abundant.

KEY WORDS

diffuse attenuation coefficient, photosynthetically active radiation, light availability, turbidity, light attenuation, K_d, K_{dPAR}

SFEWS Volume 21 | Issue 4 | Article 5

https://doi.org/10.15447/sfews.2023v21iss4art5

* Corresponding author email: erichardson@usgs.gov

1 US Geological Survey
California Water Science Center
Sacramento, CA 95819 USA

INTRODUCTION

Light transmission through water is a major control on primary productivity in aquatic habitats (Goldman 1968; Cloern 1987; Fisher et

al. 1999; Jassby et al. 2002; Cloern and Jassby 2012). Clearer waters increase light availability to plants and photosynthetic algae and bacteria by permitting more photosynthetically active radiation (PAR) to penetrate through the water column. As turbidity increases, PAR attenuates more rapidly, limiting the depth of PAR penetration. This light limitation can lead to successive effects, including lowering benthic and pelagic primary productivity of phototrophic algae and aquatic plants, changing the vertical distribution of phototaxic organisms (those who can move through the water column to find a suiTable PAR level) like zooplankton and other mobile species, shortening range of visibility, and altering predator and prey relationships (Cloern 1999; Vogel and Beauchamp 1999; Browman et al. 2000; Gallegos 2001; Ralph et al. 2007; Kirk 2010; Rathjen et al. 2012).

Light attenuation and penetration are most often modeled using the diffuse attenuation coefficient of PAR (K_{dPAR}), which is the rate at which light intensity decreases with depth. However, K_{dPAR} is difficult to monitor continuously because it requires measurements of PAR at multiple water depths. Instead, K_{dPAR} can be estimated by empirical models that contain biogeochemical parameters measured at the surface level which influence light attenuation and can be monitored continuously. By producing continuous K_{dPAR} estimates, light-attenuation values can then be used to estimate euphotic depth (Z_{eu}) and can be added into phytoplankton-productivity and habitat-suitability models that rely on this difficult-to-measure constant (e.g., Cloern 1987; Jassby et al. 2002).

Commonly, models used to estimate K_{dPAR} are based on open-ocean environments with the assumption that phytoplankton biomass (measured by chlorophyll fluorescence [fChl]) is the strongest factor that attenuates light (Morel 1988; Claustre and Maritorena 2003). Using open-ocean models in more turbid inland waters underestimates light attenuation from high suspended matter content and light absorption by dissolved organic matter (DOM; measured as fluorescent dissolved organic matter, fDOM; Cloern 1987; Saulquin et al. 2013). Additionally, in complex hydrologic systems, such as estuaries with large anthropogenic influences, like the Sacramento–San Joaquin River Delta (the Delta), a host of biogeochemical parameters that absorb and/or scatter light—e.g., terrestrial and aquatic detrital material, aeolian material, watershed-derived and bed sediments, phytoplankton, and various chemical components within runoff and effluent, among others—amplified by seasonality, geographical location, and weather patterns, can influence K_{dPAR}. To predict K_{dPAR} more accurately in such complex environments, a multivariate approach—one that accounts for several constituents, not just fChl—should be tested.

The two main factors that control light attenuation through the water column are scattering by suspended particles and absorption by DOM (Mobley 1994; Downing et al. 2012). Water with greater concentrations of suspended particulates scatters more light than clearer water. Examples of environmental and landscape factors that contribute to increased suspended particulates include runoff after rain events, increased flow velocity, algal blooms, and erosion. Suspended particles in aquatic habitats comprise mineralic sediments, algae, bacteria, and organic detritus. In aquatic systems where there is low absorption (e.g., high inorganic matter and low DOM), K_{dPAR} can display a linear relationship with turbidity (Walmsley et al. 1980; Lloyd et al. 1987). However, when absorption by DOM is substantial, the relationship between K_{dPAR} and turbidity becomes more variable (Kirk 1985). Modeling K_{dPAR} as a function of suspended sediment and DOM could provide more accurate estimates than a model that requires only suspended particle concentration measurements in systems with high DOM levels (Davies–Colley and Smith 2001). Recent estuarine models have recognized the need for a new approach to modelling K_{dPAR}, including accounting for parameters such as salinity, temperature, and particulate organic matter from the dynamics observed between particle compositions effect on absorption and scattering (Xu et al. 2005; Rose et al. 2019; Stumpner et al. 2020).

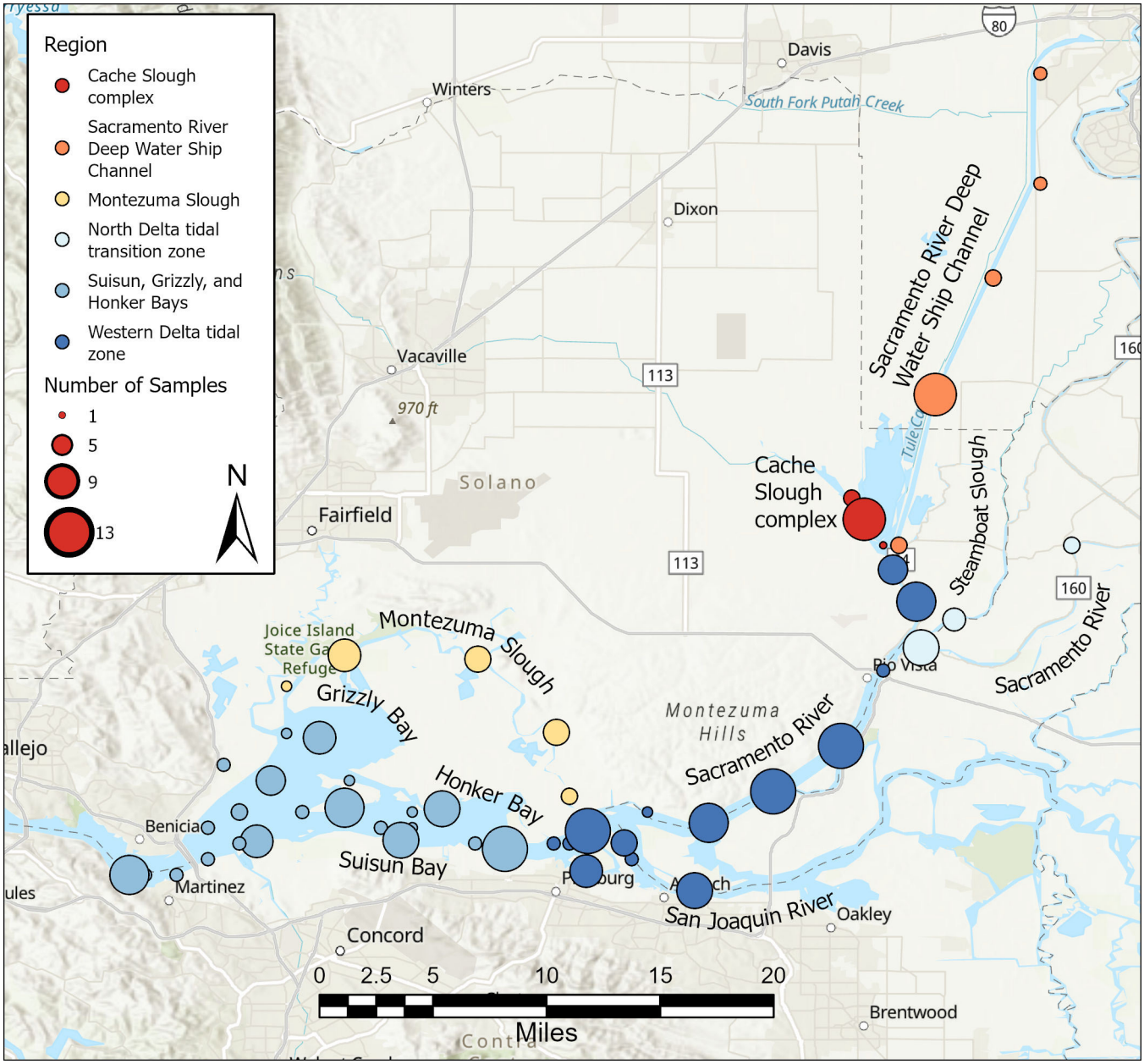

Figure 1 Sampling locations in the Sacramento–San Joaquin River Delta colored by region and sized by number of samples per site over the course of the study

MATERIALS AND METHODS

We collected depth profiles of PAR from which K_{dPAR} values were calculated at multiple locations of the Delta, which represented a range of biogeochemical and hydrologic conditions (O'Donnell et al. 2023a). We also concurrently collected *in situ* surface-water-quality parameters to characterize the concentration of particles, phytoplankton, and DOM as well as ancillary water-quality information. We assessed a variety of models at the regional and at the whole-Delta scale, as well as by season and annually, to identify the most parsimonious and robust K_{dPAR} model.

Data collection occurred across 53 sampling sites in total (Figure 1) between January of 2013 and May of 2014. Six unique regions within the Delta can be used to group the sampling sites: the Cache Slough complex; the Sacramento River

https://doi.org/10.15447/sfews.2023v21iss4art5

Deep Water Ship Channel; Montezuma Slough; North Delta tidal transition zone; Suisun, Grizzly and Honker bays; and the western Delta tidal zone (Figure 1). Each geographic region presents unique biogeochemical and hydrologic properties (Richardson et al. 2023) which may influence PAR differently. To test for differences between geographic regions, we used these regions as a categorical variable in the model selection data set.

We attached a PAR Sensor (HyperOCR I Radiometer, WET Labs, Inc., Philomath, Oregon 97370 USA) during the 2013 sampling, and later an LI-192 Underwater Quantum Sensor (LI-COR Biosciences, Lincoln, Nebraska 68504 USA) during the 2014 sampling to a weighted mount, and lowered it through the water column, recording PAR every half meter until it reached 0 (μmol $s^{-1}m^{-2}$) or until it reached a depth of 3.5 meters, whichever came first. HyperOCR I radiometer data were logged to an external data logger (Data Handler (DH4), WET Labs, Inc., Philomath, Oregon 97370 USA) and LI-192 Underwater Quantum Sensor data were collected using readings displayed on an LI-250 portable light meter (LI-COR Biosciences, Lincoln, Nebraska 68504 US). K_{dPAR} is the slope of natural log-transformed PAR measurements (μmol $s^{-1}m^{-2}$) vs. measurement depth (meters; Kirk 2010), which we calculated from the PAR sensor profiling.

An EXO2 Multiparameter Sonde (EXO2; YSI Inc., Yellow Springs, Ohio 45387 USA) was used to measure surface-water (~2 m in depth) constituents during PAR sampling, including turbidity in Formazin Nephelometric Units (FNU), water temperature (WT) in Celsius (°C), pH, fChl in μg L^{-1}, salinity in PSU, and fDOM in quinine sulfate units (QSU). The EXO2 was set up to log data internally.

Matrix tests performed by the US Geological Survey (USGS) in cooperation with Xylem indicated that EXO2 fDOM sensors produced before June 2017 had a linearity issue. We corrected fDOM data using the following formula provided by Xylem and validated by the USGS, where fDOM*uncorr* is raw sensor data and fDOM*corr* is the corrected data (2023 email between S. Smith and ETR, unreferenced, see "Notes"):

$$\mathrm{fDOM}_{corr} = \left(\frac{1}{1.035}\right)\mathrm{fDOM}_{uncorr} + 100\left(1 - \frac{1}{1.035}\right) \quad \text{Eq 1}$$

According to the unreferenced correction guidance, values below 15 QSU (n=108) are "uncorrectable" and, as such, we removed them from the data set. Afterward, we applied site-specific temperature, turbidity, and inner-filter-effect corrections to remaining fDOM concentration data (Watras et al. 2011; Downing et al. 2012). We also applied site-specific temperature corrections to EXO2 fChl concentration data (Watras et al. 2017).

In addition to utilizing sensor measurements, we gathered open-sourced environmental data to be included as potential predictors in the model. Daily average of incident solar radiation (SR) in watts per square meter (CIMIS 2021) was added into the data set because of its likelihood to influence light availability in water (Jassby 2008). The California Irrigation Management Information System (CIMIS) continuous monitoring station at Twitchell Island (station 140; Figure 1) was used as the site location for SR because of its data completeness and central location within the Delta (CIMIS 2021). The final two variables were the running sum of precipitation (RSP) in millimeters (mm) and the running sum of average daily air temperature by water year in °C (RSAT). We added these two calculated variables as proxies to account for influential seasonal and climatic trends specific to the Delta.

Briefly, the Delta is in a Mediterranean climate that can be split into two broad weather-pattern groupings each year: wet and dry periods. Dry periods begin in the spring, generally around June, and span through a hot and dry summer, extending into October. Fall is the culmination of the dry period in the Delta, with intermittent rains beginning in November. An important climatic delineation often incorporated into

environmental studies in the Delta is "water year type." Interagency managers and scientists in the Delta consider a water year to begin the previous October and extend through the end September of that calendar year, e.g., water year 2023 would be October 2022 through September 2023. The state of California classifies a "water-year type" based on the total amount of unimpaired runoff in million acre-feet within a water year for both the Sacramento and San Joaquin valleys (CDEC 2021). The five categories of water year type include, in order of decreasing runoff: wet, above normal, normal, dry, and critical. Both valleys have different metrics for classifying water-year type and can differ within the same water year (CDEC 2021). This study took place across 2 water years (2013 and 2014) which had water year type designations of dry and critical for the Sacramento Valley and critical and critical for the San Joaquin Valley. Although the Delta extends into both valleys, environmental studies taking place in the Delta generally refer to metrics collected in Sacramento Valley because it is more influential on Delta water quantity and quality. Running sum of precipitation was used as a proxy for both water-year type and wet- or dry-season delineation. Running sum of precipitation might be especially useful for real-time calculations where final water-year type is unknown and therefore cannot be entered into the model as a categorical variable. Running sum of air temperature for use as a proxy for position in time with respec to the water year. The Twitchell Island continuous monitoring station was also used for the RSP and RSAT data (station 140; CIMIS 2021; Figure 1).

Model Selection

We explored several data types to develop and assess our models: *in situ* measurements of turbidity, fDOM and chlorophyll; the water quality variables salinity, water temperature, and pH, as well as indicators of environmental conditions, such as SR, RSP, and RSAT. To find and remove covariable parameters, we performed a stepwise removal of parameters with a variance inflation factor (VIF) cutoff of 2.5 using the 'car' package (Fox and Weisberg 2019) in R (R Core Team 2021) with the data set that contained each testing variable (Figure 2; Kassambara 2019; and including sub-region), excluding any record where fDOM concentration was null because of sensor corrections.

Variance inflation factor testing resulted in the successive removal of RSAT, sub-region, SR, RSP, and finally fDOM. Because the literature review suggested that fDOM was among the most important factors that influenced light attenuation (in addition to turbidity and fChl; e.g., Cloern 1987; Saulquin et al. 2013), we decided to keep fDOM in the data set to develop the initial model. We ran a stepwise regression with backward removal using the 'caret' R package (Kuhn 2021), which resulted in the most performant model (smallest mean-squared error) that contained turbidity only. Because fDOM was not included in the best-performing model, and because it led to collinearity issues and data loss, we determined that the records which were removed as a result of null fDOM concentrations should be brought back into the testing data frame, and that fDOM should not be included in the final testing data set.

We brought all testing parameters (with the exception of fDOM) back into the data set, including those initially removed as a result of null fDOM concentration measurements, and we repeated VIF testing (n=242). This resulted in the successive removal of sub-region, RSP, and SR. The final data set we used to select the model included turbidity, fChl, WT, RSAT, pH, and salinity. We repeated the stepwise regression with backward removal to select the final input parameters to the model. The top-performing model contained turbidity only. Using the turbidity-only model, we removed seven outliers where Cook's distance was greater than three times the mean of the Cook's distance for the data set during assumptions testing, and then calculated the model coefficients and statistics.

Model Demonstration Data Set

To test the functionality of the model, we applied the formula to two open-sourced demonstration data sets that contained turbidity in FNU; one spatially rich and one temporally rich.

https://doi.org/10.15447/sfews.2023v21iss4art5

The spatially rich data set consisted of a high-resolution mapping survey which spanned the Delta (Bergamaschi et al. 2020). This mapping data set represents three "snapshots" in time, with surveys occurring in May, July, and October of 2018, each lasting 3 days. The temporally rich data set consisted of 6 months of tidally filtered (Godin 1972) turbidity data in FNU collected at the USGS Grizzly Bay continuous monitoring station (Figure 1; USGS station number 380631122032201; USGS 2023; *http://waterdata.usgs.gov/usa/nwis*).

For both sets of demonstration data, we estimated K_{dPAR} using turbidity measurements (FNU). Each mapping survey overlapped in time and location with the continuous monitoring station data set. For comparison, we used only mapping data collected within Grizzly Bay (Figure 1) to compare to time-series data collected at the Grizzly Bay continuous monitoring station. Mapping data were collected at a frequency of one measurement per second per parameter, whereas time-series data were collected every 15 min. This difference in frequency of measurements resulted in few records overlapping each survey at the Grizzly Bay continuous monitoring station ($n=3$ for continuous monitoring station data collected during the May and July 2018 Delta mapping survey, $n=1$ during the October 2018 survey, and $n>1{,}300$ for each mapping survey while the boat was collecting data within Grizzly Bay).

Data used for each presented model demonstration and comparison (turbidity [FNU], and chlorophyll fluorescence [µg L^{-1}]) were averaged within datasets to obtain one value per parameter per survey. Daily solar radiation in watts per m^2 was obtained from the Twitchell Island continuous monitoring station (station 140; CIMIS 2021; Figure 1).

Where data were comparable, we used the present turbidity-only model to calculate K_{dPAR}. We then used our K_{dPAR} estimates in established euphotic-depth (Kirk 2010) and primary- productivity (Jassby et al. 2002) models, comparing mapping to time-series predictions.

Table 1 Average Turbidity (FNU) and chlorophyll fluorescence (fChl; µg L^{-1}) estimates at the USGS Grizzly Bay continuous monitoring station during the May, July, and October Delta mapping surveys, and near the same monitoring station using the Delta mapping survey data, and daily solar radiation (SR; watts m−2) at the Twitchell Island continuous monitoring station (station 140; CIMIS 2021; Figure 1)

	Grizzly Bay continuous monitoring station Data		Delta mapping data collected within Grizzly Bay		Twitchell Island continuous monitoring station
Date	Turbidity (FNU)	fChl (µg L^{-1})	Turbidity (FNU)	fChl (µg L^{-1})	SR (watts m^{-2})
05/17/2018	111.00	13.62	106.77	18.46	341
7/26/2018	81.66	4.42	64.05	3.44	321
10/17/2018	18.06	2.08	8.52	2.15	185

RESULTS

The final K_{dPAR} model showed a high predictive power ($R^2=0.91$, RSE=0.28, $p<0.0001$, df=234, F=2406; Figures 3 and 4). Overall, K_{dPAR} was most highly correlated with turbidity, followed by fDOM and fChl (Figure 2), each with a positive relationship. A slight positive correlation between SR and K_{dPAR} is evident, as well as a slight negative relationship between pH and K_{dPAR} (Figure 2). This correlation generally means that the greater the turbidity, fDOM, and fChl concentrations, the greater the attenuation of PAR. Water temperature, RSP, RSAT, and salinity did not each appear to be correlated with K_{dPAR}. It is unclear if these relationships hold true throughout the Delta, or if small regional shifts occur.

$$K_{dPAR} = 0.52 + (Turbidity * 0.11) \quad \text{Eq 2}$$

The final K_{dPAR} model is as follows:

Turbidity values used to create the final model ranged from 1.24 to 45.17 FNU, the maximum fDOM value was 62.80 QSU (note that the lower range of fDOM data were deleted as a result of sensor corrections), and fChl ranged from 0.31 to 6.77 µg L^{-1}.

Model Demonstration

Using the K_{dPAR} model, we evaluated spatial and temporal changes in K_{dPAR} across the Delta. We

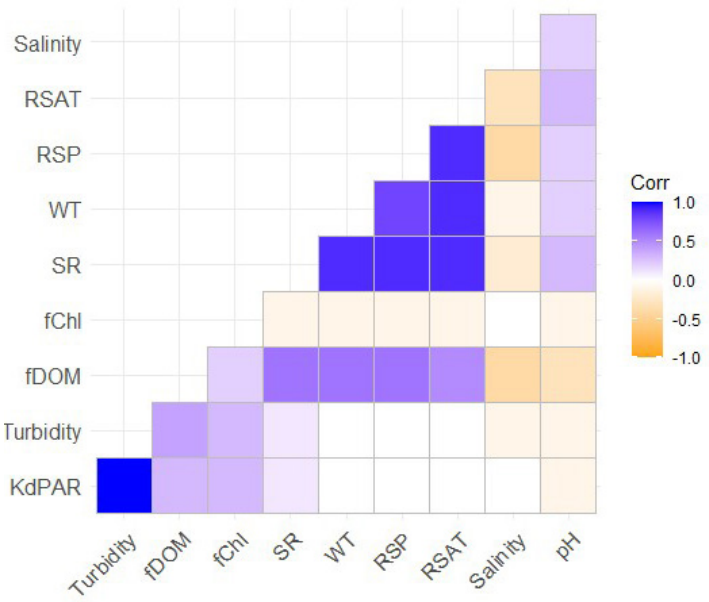

Figure 2 Correlation plot between all non-null, numeric parameters used as inputs during model testing, including the explanatory variable (the light attenuation coefficient; K_{dPAR}), and predictor variables turbidity, fluorescence of dissolved organic matter (fDOM), fluorescence of chlorophyll (fChl), solar radiation (SR), water temperature (WT), the running sum of precipitation (RSP), the running sum of air temperature (RSAT), salinity, and pH

input turbidity (FNU) data from Delta-wide water-quality mapping surveys conducted in May, July, and October of 2018 by the USGS (Bergamaschi et al. 2020) into the K_{dPAR} model equation. The results (Figure 5) depict an ability to predict K_{dPAR} granularly across the Delta. These data show particular variability within the Suisun, Grizzly, and Honker Bay region (Figures 1, 5, and 6) which is known to experience elevated and variable turbidity caused by wind–wave sediment re-suspension (Conomos and Peterson 1977; Burau et al. 2000), and thus can be expected to exhibit correspondingly elevated and variable K_{dPAR}.

We also demonstrated this model using tidally filtered (Godin 1972) turbidity (FNU) data collected at the USGS Grizzly Bay continuous monitoring station (Figure 1). Results from this temporally rich time-series data set show that K_{dPAR} varied by an order of magnitude during the mapping periods, with large excursions in K_{dPAR} occurring in a matter of days (Figure 6).

These K_{dPAR} values estimated using both demonstration data sets display similar trends (Figures 5 and 6), where K_{dPAR} decreases by survey within the Grizzly Bay area (and thus light availability increases; Tables 2 and 3). While the K_{dPAR} estimates at the Grizzly Bay continuous monitoring station and within Grizzly Bay during the three presented Delta-wide surveys show the same trend between the two data sources, the results are not identical (Table 2).

The average Delta mapping data *within* Grizzly Bay indicates lower average K_{dPAR} estimates than average K_{dPAR} estimates *at* the Grizzly Bay continuous monitoring station during the same time-frame as the mapping surveys. A likely explanation for these differences is that the continuous monitoring station represents two measurements from one location in Grizzly Bay, 15 min apart, whereas the survey data is from a much larger area within Grizzly Bay and across a larger time-frame (more than 30 min per survey).

Like K_{dPAR} estimates, we can produce Z_{eu} (depth at which 1% of surface irradiance remains) estimates across the Delta and across time wherever turbidity (FNU) data are available, using the following formulas (Kirk 2010;):

$$Z_{eu} = \frac{\ln(0.01)}{-K_{dPAR}} \quad \text{Eq 3}$$

or

$$Z_{eu} = \frac{\ln(0.01)}{-0.52 + Turbidity * 0.11} \quad \text{Eq 4}$$

Similarly, where turbidity in FNU, daily average SR in watts per m^2 (converted to E by multiplying

https://doi.org/10.15447/sfews.2023v21iss4art5

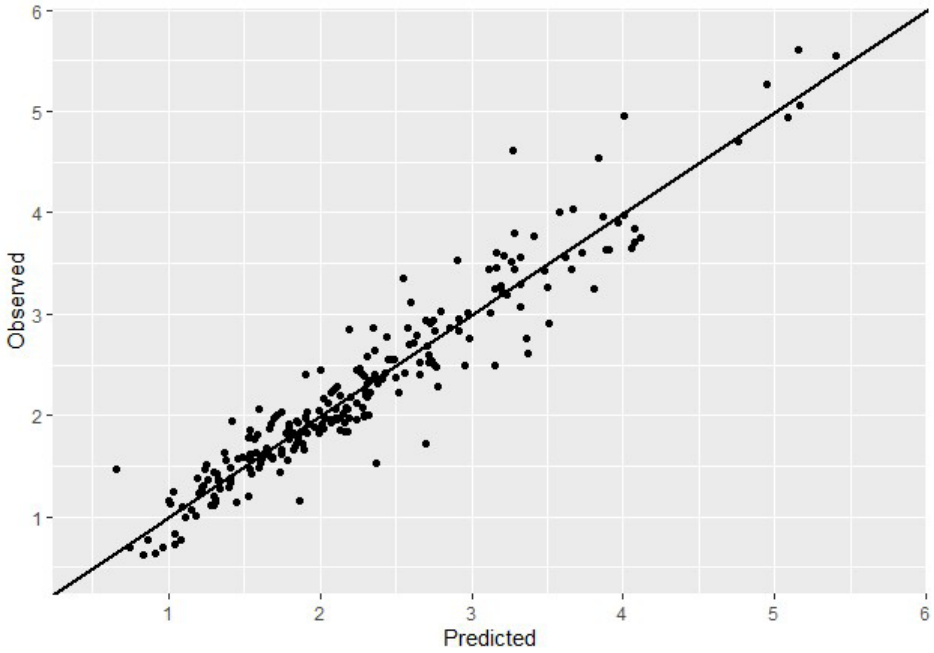

Figure 3 Plot of light attenuation coefficient (K_{dPAR}) estimates predicted by the K_{dPAR} model against observed K_{dPAR} estimates by *in situ* PAR measurements with depth

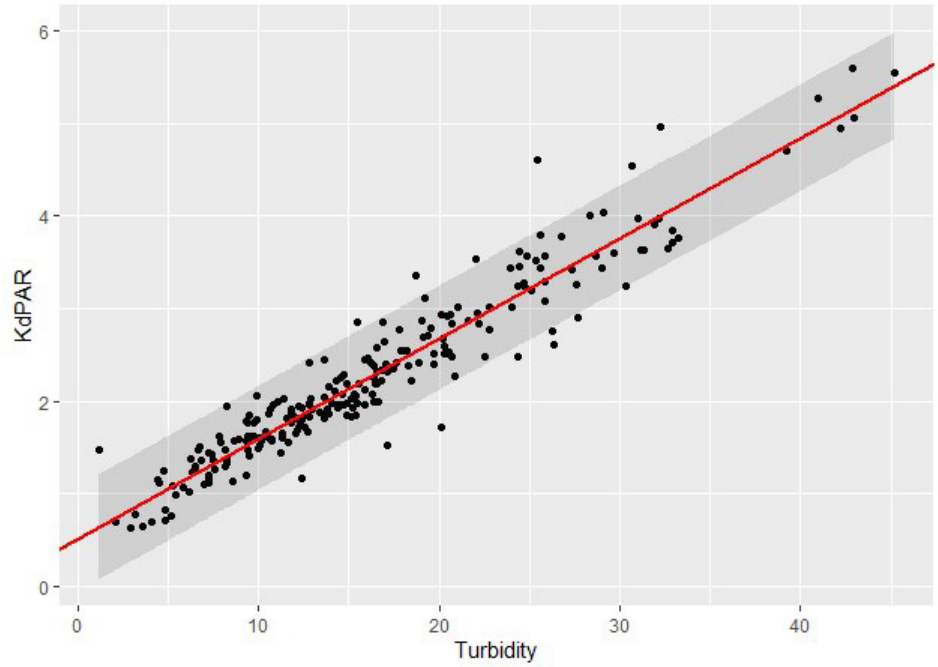

Figure 4 Plot of turbidity against K_{dPAR}, with 95% confidence bands

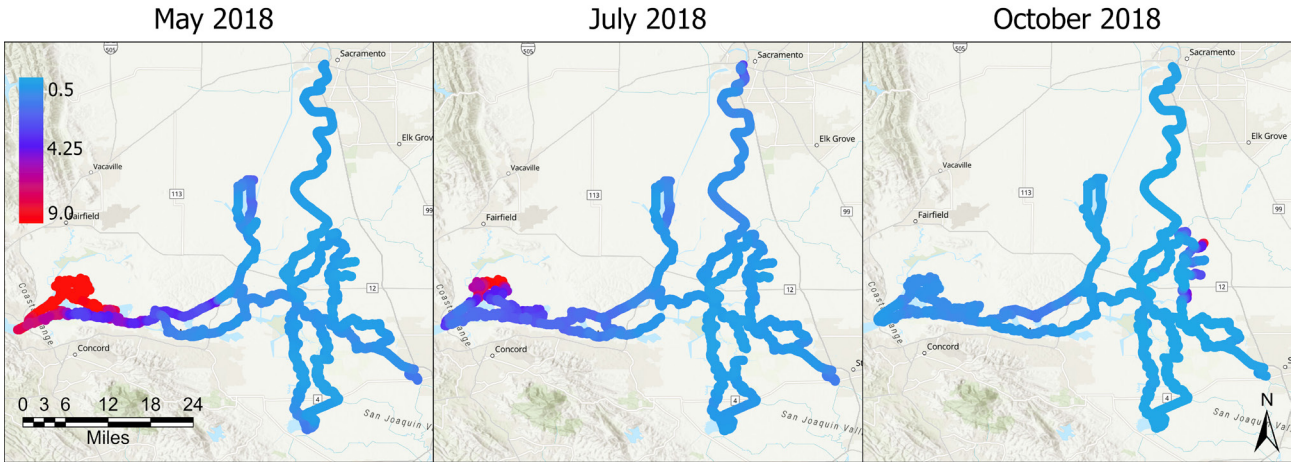

Figure 5 K_{dPAR} estimates calculated across the Sacramento–San Joaquin Delta during three boat-based, high-resolution surveys (May, July, and October) conducted in 2018 (Bergamaschi et al. 2020)

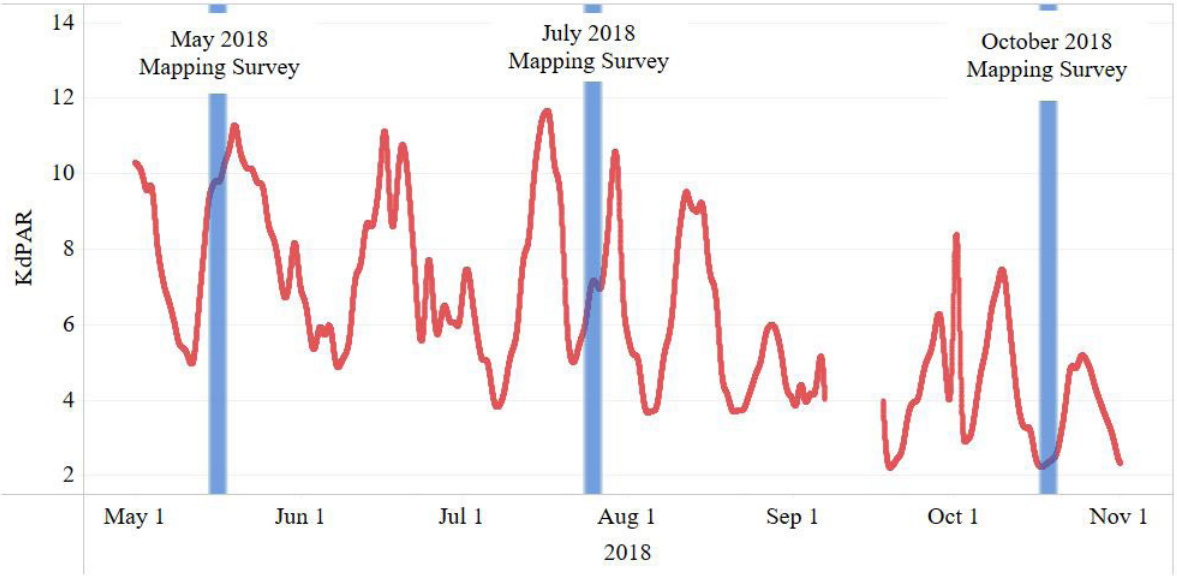

Figure 6 Continuous K_{dPAR} estimates calculated using tidally-filtered turbidity data produced by the USGS at a continuous monitoring station in Grizzly Bay, USGS station number 380631122032201. Bars represents dates where Delta-wide surveys occurred (see Figure 4).

https://doi.org/10.15447/sfews.2023v21iss4art5

Table 2 Average K_{dPAR} estimates at the USGS Grizzly Bay continuous monitoring station, station number 380631122032201, during the May, July, and October Delta mapping surveys and near the same continuous monitoring station using the Delta mapping survey data (residual standard error = 0.28).

Survey	Average K_{dPAR}	
	Grizzly Bay continuous monitoring station	Delta mapping data collected in Grizzly Bay
May 2018	12.73 ± 0.28	12.27 ± 0.28
July 2018	9.50 ± 0.28	7.57 ± 0.28
October 2018	2.51 ± 0.28	1.46 ± 0.28

Table 3 Average euphotic depth (Z_{eu}) estimates at the USGS Grizzly Bay continuous monitoring station, USGS station number 380631122032201, during the May, July, and October 2018 Delta mapping surveys and near the same continuous monitoring station using the Delta mapping survey data

Survey	Average Zeu (m)	
	Grizzly Bay continuous monitoring station	Delta mapping data collected in Grizzly Bay
May 2018	0.36	0.38
July 2018	0.51	0.66
October 2018	1.84	3.16

by a factor of 0.18; Jassby 2005), and fChl in µg L^{-1} data are available, we can estimate gross primary productivity (GPP; mg C $m^{-2} d^{-1}$; Table 4; where 0.73 is an approximately constant Delta-specific efficiency factor; Jassby et al. 2002; Equations 5 and 6).

$$GPP = 0.73 * SR * 0.18 * fChl * Z_{eu} \quad \text{Eq 5}$$

or

$$GPP = \frac{0.61 * SR * fChl}{0.52 + Turbidity * 0.11} \quad \text{Eq 6}$$

Altogether, the K_{dPAR} estimates calculated with high-resolution mapping data and continuous monitoring station turbidity data present examples of how the K_{dPAR} model can be applied to calculate habitat metrics using commonly measured parameters.

DISCUSSION

Turbid conditions, such as those found in the Delta, are thought to be the leading cause inhibiting phytoplankton growth and productivity in estuaries (Cloern 1987). This study supports this hypothesis because turbidity displayed the strongest relationship with K_{dPAR} (Figure 2). Although the nature of the runoff and discharge (e.g., comprising absorptive organic matter) that enters the Delta suggests that fDOM may influence K_{dPAR} and how turbidity affects KdPAR, Fluorescent DOM did not improve the model because it was not included in the best-performing model when included in the testing data set. Fluorescent DOM sensor corrections resulted in the deletion of all data collected at the lower end of the range of fDOM concentration measurements (< 15 QSU; n = 108). However, higher fDOM concentrations are thought to alter how turbidity affects light attenuation, so the deletion of the lower end of the fDOM measurements should not have muted that effect. Considering that fDOM was not included in the most parsimonious K_{dPAR} model, the hypothesis that fDOM affects the linearity of the relationship between K_{dPAR} and turbidity is not supported in the context of the Delta, where light absorption by fDOM may not be substantial.

Chlorophyll fluorescence was also not included in the "best-performing" multivariate model. Previous publications have concluded that chlorophyll was best suited to model K_{dPAR} in open ocean water, and turbidity and fDOM were better suited to model K_{dPAR} in nutrient-rich inland water (Cloern 1987; Morel 1988; Claustre and Maritorena 2003; Saulquin et al. 2013). Given that the Delta is estuarine, we hypothesized that fChl may be influential. However, because the highest fChl value was relatively low (6.77 µg L^{-1}), it is possible that fChl may exert a stronger influence on K_{dPAR} during periods of elevated fChl, such as during an algal bloom. Although there is no consensus on a fChl bloom condition threshold (Adams et al. 2021) because global bloom dynamics are too variable (Dai et al. 2023), fChl ranges in the Delta can certainly exceed 6.77 µg L^{-1}. One

Table 4 Average gross primary productivity (GPP) estimates at the USGS Grizzly Bay continuous monitoring station, USGS station number 380631122032201, during the May, July, and October 2018 Delta mapping surveys and near the same continuous monitoring station using the Delta mapping survey data

Survey	Average GPP (mg C m^{-2} d^{-1})	
	Grizzly Bay continuous monitoring station	Delta mapping data collected in Grizzly Bay
May 2018	209	302
July 2018	92	94
October 2018	93	165

USGS survey completed in the spring of 2020 reported over 400 µg L^{-1} in a dead-end slough as measured by a Fluoroprobe III (bbe Moldaenke, Kiel, Germany; O'Donnell et al. 2023b), although median springtime highs rarely exceed 10 µg L^{-1} (Bergamaschi et al. 2020; O'Donnell at al. 2023b). Although turbidity sensors pick up light scattered by phytoplankton, we recommend that users of this model exercise caution when applying the formula to data collected during an algal bloom. The light absorbed or blocked by phytoplankton during a bloom might become more influential than turbidity at a high concentration. Research to determine the threshold at which this relationship changes would be beneficial.

A light-attenuation model for Chesapeake Bay created by Xu et al. (2005) was used to determine that chlorophyll-*a* concentration did not highly influence light attenuation. They did not provide ranges of values used within their testing data; however, they did highlight the value of producing different models that used different conditions. Specifically, Xu et al. (2005) separated their model by salinity (as a proxy for fDOM). Although our Delta study lacks a low range in fDOM concentration measurements from sensor corrections, the model did not appear to require partitioning because the R^2 value is 0.91 using turbidity only, even though the presumably low-fDOM samples were included. However, because Xu et al. (2005) recognized a salinity break, we caution users against extending this model into the highly brackish waters of the San Francisco Bay (bay). Conducting a study similar to our study in the bay and creating a bay-specific K_{dPAR} model would better describe how salinity and fChl influence KdPAR further downstream into the estuary. The Xu et al. (2005) model demonstrated that total suspended solid concentration (like turbidity) was the major attenuator of light in Chesapeake Bay. Similarly, turbidity is the largest local attenuator of light in the Delta, perhaps overshadowing any effect by fChl or fDOM.

Ultimately, a relationship among seasonal or weather patterns and K_{dPAR} was not observed in the Delta. and this was unexpected because of the strong seasonality of light-attenuating substances reported in another Chesapeake Bay model (Rose et al. 2019). Attenuation values were high in the spring and decreased through summer and fall (Figure 6; Table 2), supporting the idea that seasonally lower flows result in lower suspended sediments. Attenuation values were lowest in the fall before increased precipitation restored flow and decreased attenuation (Figure 6; Table 2). Initially, parameters from open-sourced data sets that were meant to act as seasonal and weather-pattern proxies (RSP and RSAT) were removed from the model-selection process because they covaried with other input parameters (perhaps WT; Figure 2). However, when the VIF testing was repeated using the larger data set (reinserting records previously removed as a result of fDOM corrections and removing fDOM from the testing data set), RSAT did not covary enough to be removed from the data set used to select the K_{dPAR} model. Because data were not collected evenly across season or water-year type, ground-truthing in rainier years (e.g., where water-year type is not dry or critical as in the presented data) and in summer months (model tuning data were not collected in June–August for this study) might add value to understanding how the model performs in different conditions. Ultimately, we included neither RSAT or WT in the final model, and neither was WT. Although seasonal and weather patterns influence light availability, turbidity measurements accounted for these relationships.

Similarly, we removed the categorical regional variable from both iterations of the model testing data set because of covariation. Similar

https://doi.org/10.15447/sfews.2023v21iss4art5

to seasonal and weather effects, the relationship between turbidity and K_{dPAR} did not vary substantially among different locations within the Delta, even though measured turbidity varied substantially throughout the Delta.

Estimates of Z_{eu} and K_{dPAR} presented in this paper depended only on turbidity, but GPP was also a function of fChl and SR. Unlike Z_{eu} and K_{dPAR}, GPP estimates did not follow a consistent stepwise trend across months (Tables 2 through 4), even though each input parameter used to compute GPP followed a consistent stepwise trend across months (Table 1). This demonstration underscored that trends in data may be similar, but the contributions and ratios of internal, external, and environmental factors that influence the Delta resulted in a more complex relationship between GPP and water quality.

The K_{dPAR} model presented here can be applied broadly throughout the Delta because the model only includes one commonly measured input variable (turbidity). Connecting real-time surface-level turbidity data from sensors located throughout the Delta allows K_{dPAR} to be estimated at high temporal resolution (see Figure 6). Special studies that involve collecting turbidity measurements may also benefit from this model, since it offers the possibility of estimating K_{dPAR} at a high spatial resolution (see Figure 5). These newly available K_{dPAR} estimates can be used to improve estimates of productivity throughout the Delta, and to improve other water-quality models (Cloern 1987; Jassby et al. 2002; Lee et al. 2021).

CONCLUSIONS

Open-ocean models place high importance on phytoplankton (measured by fChl) as a controlling factor of light attenuation, but inland-water-body models have used parameters such as turbidity and fDOM to model light attenuation. Despite the expectation that accurately modeling K_{dPAR} would require us to account for light attenuation by phytoplankton, dissolved organic matter, and turbidity, we found that a model using only turbidity had the smallest mean-squared error. Because the best-performing model contained turbidity only, the hypothesis that inland waters require different light-attenuation models than open-ocean waters is supported. However, within the Delta, fDOM does not appear to affect turbidity's influence on K_{dPAR}. It is unclear how this relationship would change if measurements were collected farther seaward, or if there is a cutoff point at which fChl becomes a more important or even primary constraint.

Neither regional nor seasonal effects were significant variables in the presented model, making the model broadly applicable to Delta-wide forecasting. K_{dPAR} estimates obtained from this model may serve many purposes, such as predicting phytoplankton productivity, euphotic depth, habitat suitability, and water quality, among others. Real-time sensor measurements for turbidity (and ancillary measurements required for primary productivity estimates, e.g., fChl and SR) are now available through many monitoring networks (e.g., USGS, Bureau of Reclamation, San Francisco Estuary Institute, California Department of Water Resources). Incorporating these real-time data into the presented model would facilitate creation of a network of continuous K_{dPAR} predictions across the Delta, , which could help apply hindcasting and forecasting to habitat conditions and primary productivity.

ACKNOWLEDGMENTS

This study was funded by the US Bureau of Reclamation. We thank Brock Huntsman for useful inputs to statistical analyses, as well as Bryan Downing for largely contributing to the design of the field work. Many people were involved in field data collection, including Amy Story, Travis von Dessonneck, Scott Nagel, Brian Husong, and Mike Sauer. We also thank Brendan Wakefield and Michael Hitzelberger for assistance retrieving data used in the model selection and demonstration data set testing, and Andrea Jaegge for useful input to the discussion. Finally, we thank Dan Killam for providing feedback on an earlier version of this manuscript. Any use of trade, firm, or product names is for descriptive

purposes only and does not imply endorsement by the US Government.

REFERENCES

Adams H, Ye J, Persaud B, Slowinski S, Kheyrollah Pour H, Van Cappellen P. 2021. Chlorophyll-*a* growth rates and related environmental variables in global temperate and cold-temperate lakes. Earth Syst. Sci. Data [accessed 2023 Mar 15]. *https://doi.org/10.5194/essd-2021-329*

Bergamaschi BA, Kraus TEC, Downing BD, Soto Perez J, O'Donnell K, Hansen JA, Hansen AM, Gelber AD, Stumpner EB. 2020. Assessing spatial variability of nutrients and related water quality constituents in the California Sacramento–San Joaquin Delta at the landscape scale: 2018 high resolution mapping surveys. US Geological Survey data release. [accessed 2023 Mar 15]. *https://doi.org/10.5066/P9FQEUAL*

Browman HI, Rodriguez CA, Beland F, Cullen JJ, Davis RF, Kouwenberg JHM, Kuhn PS, McArthur B, Runge JA, St–Pierre JF, et al. 2000. Impact of ultraviolet radiation on marine crustacean zooplankton and ichthyoplankton: a synthesis of results from the estuary and gulf of St. Lawrence, Canada. Mar Ecol Prog Ser. [accessed 2023 Mar 15];199:293–311. *https://doi.org/10.3354/meps199293*

Burau JR, Monismith SG, Stacey MT, Oltmann RN, Lacy J, Schoellhamer DH. 2000. Recent research on the hydrodynamics of the Sacramento–San Joaquin River Delta and North San Francisco Bay. IEP Newsletter. [accessed 2023 Mar 15];11(2):45–55. Available from: *https://pubs.er.usgs.gov/publication/70174259*

[CDEC] California Data Exchange Center. 2021. Chronological reconstructed Sacramento and San Joaquin Valley water year hydrologic classification indices. Department of Water Resources California Cooperative Snow Surveys. [accessed 2023 Mar 15]. Available from: *https://cdec.water.ca.gov/reportapp/javareports?name=WSIHIST*

[CIMIS] California Irrigation Management Information System. 2021. CIMIS station reports. California Department of Water Resources. [accessed 2023 Mar 15]. Available from: *https://cimis.water.ca.gov/Stations.aspx*

Claustre H, Maritorena S. 2003. The many shades of ocean blue. Science. [accessed 2023 Mar 15];302(5650):1514–1515. *https://doi.org/10.1126/science.1092704*

Cloern JE. 1987. Turbidity as a control on phytoplankton biomass and productivity in estuaries. Cont Shelf Res. [accessed 2023 Mar 15];7(11–12):1367–1381. *https://doi.org/10.1016/0278-4343(87)90042-2*

Cloern JE. 1999. The relative importance of light and nutrient limitation of phytoplankton growth: a simple index of coastal ecosystem sensitivity to nutrient enrichment. Aquat Ecol. [accessed 2023 Mar 15];33:3–15. *https://doi.org/10.1023/A:1009952125558*

Cloern JE, Jassby AD. 2012. Drivers of change in estuarine–coastal ecosystems: discoveries from four decades of study in San Francisco Bay. Rev Geophys. [accessed 2023 Mar 15];50(4). *https://doi.org/10.1029/2012rg000397*

Conomos TJ, Peterson DH. 1977. Suspended particle transport and circulation in San Francisco Bay: an overview. In: Wiley M, editor. Estuarine processes. New York (NY): Academic Press. [accessed 2023 Mar 15]. p. 82–97. *https://doi.org/10.1016/B978-0-12-751802-2.50014-X*

Dai Y, Yang S, Zhao D, Hu C, Xu W, Anderson DM, Li Y, Song X–P, Boyce DG, Gibson L, et al. 2023. Coastal phytoplankton blooms expand and intensify in the 21st century. Nature. [accessed 2023 Mar 15];615:280–284 *https://doi.org/10.1038/s41586-023-05760-y*

Davies–Colley RJ, Smith DG. 2001. Turbidity, suspended sediment, and water clarity: a review. J Am Water Resour Assoc. [accessed 2023 Mar 15];37(5):1085–1101. *https://doi.org/10.1111/j.1752-1688.2001.tb03624.x*

Downing BD, Pellerin BA, Bergamaschi BA, Saraceno JF, Kraus TEC. 2012. Seeing the light: the effects of particles, dissolved materials, and temperature on *in situ* measurements of DOM fluorescence in rivers and streams. Limnol Oceanogr–Meth. [accessed 2023 Mar 15];10:767–775. *https://doi.org/10.4319/lom.2012.10.767*

Fisher TR, Gustafson AB, Sellner K, Lacouture R, Haas LW, Wetzel RL, Magnien R, Everitt D, Michaels B, Karrh R. 1999. Spatial and temporal variation of resource limitation in Chesapeake Bay. Mar Biol. [accessed 2023 Mar 15];133(4):763–778. *https://doi.org/10.1007/s002270050518*

Fox J, Weisberg S. 2019. An R companion to applied regression. 3rd ed. Thousand Oaks (CA): Sage. 608 p. [accessed 2022 Nov 14]. Available from: *https://socialsciences.mcmaster.ca/jfox/Books/Companion/*

Gallegos CL. 2001. Calculating optical water quality targets to restore and protect submersed aquatic vegetation: overcoming problems in partitioning the diffuse attenuation coefficient for photosynthetically active radiation. Estuaries. [accessed 2023 Mar 15];24(3):381–397. *https://doi.org/10.2307/1353240*

Godin G. 1972. The analysis of tides. Toronto (Ontario): University of Toronto Press. p. 1–264.

Goldman, Charles R. 1968. Aquatic primary production. Am Zool. 8(1):31–42.

Jassby AD. 2005. Phytoplankton regulation in a eutrophic tidal river (San Joaquin River, California). San Franc Estuary Watershed Sci. [accessed 2023 Mar 15];3(1). *https://doi.org/10.15447/sfews.2005v3iss1art5*

Jassby AD. 2008. Phytoplankton in the upper San Francisco Estuary: recent biomass trends, their causes, and their trophic significance. San Franc Estuary Watershed Sci. [accessed 2023 Mar 15];6(1). *https://doi.org/10.15447/sfews.2008v6iss1art2*

Jassby AD, Cloern JE, Cole BE. 2002. Annual primary production: patterns and mechanisms of change in a nutrient-rich tidal ecosystem. Limnol Oceanogr. [accessed 2023 Mar 15];47(3):698–712. Availabe from: *https://www.jstor.org/stable/3069158*

Kassambara A. 2019. ggcorrplot: visualization of a correlation matrix using 'ggplot2.' [accessed 2023 Mar 15]. Available from: *https://cran.r-project.org/web/packages/ggcorrplot/index.html*

Kirk JT. 1985. Effects of suspensoids (turbidity) on penetration of solar radiation in aquatic ecosystems. Hydrobiologia. [accessed 2023 Mar 15];125:195–208. *https://doi.org/10.1007/BF00045935*

Kirk JT. 2010. Light and photosynthesis in aquatic ecosystems. 3rd edition. Cambridge (England): Cambridge University Press. [accessed 2023 Mar 15]. p.1–649. *https://doi.org/10.1017/CBO9781139168212*

Kuhn M. 2021. caret: classification and regression training. ver 6.0-93. [accessed 2023 Mar 15]. Available from: *https://CRAN.R-project.org/package=caret*

Lee CM, Hestir EL, Tufillaro N, Palmieri B, Acuña S, Osti A, Bergamaschi BA, Sommer T. 2021. Monitoring turbidity in San Francisco Estuary and Sacramento–San Joaquin Delta using satellite remote sensing. J Am Water Resour Assoc. [accessed 2023 Mar 15];57(5):737–751. *https://doi.org/10.1111/1752-1688.12917*

Lloyd DS, Koenings JP, La Perriere JD. 1987. Effects of turbidity in fresh waters of Alaska. N Am J Fish Manag. [accessed 2023 Mar 15];7:18–33. *https://doi.org/10.1577/1548-8659(1987)7<18:EOTIFW>2.0.CO;2*

Mobley CD. 1994. Light and water: radiative transfer in natural waters. Academic Press. [accessed 2023 Mar 15]. p. 1-592. Available from: *https://www.oceanopticsbook.info/view/introduction/level-2/other-web-resources*

Morel A. 1988. Optical modeling of the upper ocean in relation to its biogenous matter content (case I waters). J Geophys Res–Oceans. [accessed 2023 Mar 15];93(C9):10749–10768. *https://doi.org/10.1029/JC093iC09p10749*

O'Donnell, K, Richardson ET, Bergamaschi, BA. 2023a. K_{dPAR} and surface water-quality data collected in the Sacramento–San Joaquin River Delta in 2013 and 2014. US Geological Survey data release. [accessed 2023 Nov 30]. *https://doi.org/10.5066/P9N8GV23*

O'Donnell K, Stumpner E, Richardson ET, Soto Perez J, Sturgeon CL, Delascagigas A, Nakatsuka K, Uebner MQ, Bergamaschi T, Hansen JA, et al. 2023b. Assessing spatial variability of nutrients, phytoplankton and related water-quality constituents in the California Sacramento–San Joaquin Delta at the landscape scale: 2020–2021 high-resolution mapping surveys. US Geological Survey data release. [accessed 2023 Mar 15]. *https://doi.org/10.5066/P90VYUBX*

R Core Team. 2021. R: a language and environment for statistical computing. Vienna (Austria): R foundation for statistical computing. [accessed 2023 Mar 15]. Available from: *https://www.R-project.org/*

Ralph PJ, Durako MJ, Enriquez S, Collier CJ, Doblin MA. 2007. Impact of light limitation on seagrasses. J Exp Mar Biol Ecol. [accessed 2023 Mar 15];350:176–193. *https://doi.org/10.1016/j.jembe.2007.06.017*

Rathjen KA, Breitburg DL, Neale PJ. 2012. Effects of ultraviolet radiation on the growth, reproduction and survival of the lobate ctenophore *mnemiopsis leidyi* in Chesapeake Bay. J Exp Mar Biol Ecol. [accessed 2023 Mar 15];432:121–130. *https://doi.org/10.1016/j.jembe.2012.06.029*

Richardson ET, Bouma–Gregson K, Kraus TEC, O'Donnell K, Sturgeon CL, Soto Perez J, Delascagigas A, Nakatsuka KK, Burau DJ, Gelber AD, et al. 2023. Phytoplankton species composition and abundance in the Sacramento–San Joaquin River Delta: microscopic enumeration of USGS samples, beginning in 2016. US Geological Survey data release. [accessed 2023 Jun 22]. *https://doi.org/10.5066/P97ZBPLH*

Rose KC, Neale PJ, Tzortziou M, Gallegos CL, Jordan TE. 2019. Patterns of spectral, spatial, and long-term variability in light attenuation in an optically complex sub-estuary. Limnol Oceanogr. [accessed 2023 Mar 15];64(S1):S257–S272. *https://doi.org/10.1002/lno.11005*

Saulquin B, Hamdi A, Gohin F, Populus J, Mangin A, D'Andon OF. 2013. Estimation of the diffuse attenuation coefficient k_{dPAR} using MERIS and application to seabed habitat mapping. Remote Sens Environ. [accessed 2023 Mar 15];128:224-233. *https://doi.org/10.1016/j.rse.2012.10.002*

Stumpner EB, Bergamaschi BA, Kraus TEC, Parker AE, Wilkerson FP, Downing BD, Dugdale RC, Murrell MC, Carpenter KD, Orlando JL et al. 2020. Spatial variability of phytoplankton in a shallow tidal freshwater system reveals complex controls on abundance and community structure. Sci Total Environ. [accessed 2023 Mar 15];700: 134392. *https://doi.org/10.1016/j.scitotenv.2019.134392*

[USGS] US Geological Survey. 2023. USGS water data for the nation: National Water Information System. [accessed 2023 Mar 15]. *https://doi.org/10.5066/F7P55KJN*

Vogel JL, Beauchamp DA. 1999. Effects of light, prey size, and turbidity on reaction distances of Lake Trout (*salvelinus namaycush*) to salmonid prey. Can J Fish Aquat Sci. [accessed 2023 Mar 15];56(7):1293–1297. *https://doi.org/10.1139/cjfas-56-7-1293*

Walmsley RD, Butty M, Van Der Piepen H, Grobler D. 1980. Light penetration and the interrelationships between optical parameters in a turbid subtropical impoundment. Hydrobiologia. [accessed 2023 Mar 15];70:145–157. *https://doi.org/10.1007/bf00015500*

Watras CJ, Hanson PC, Stacy TL, Morrison KM, Mather J, Hu YH, Milewski P. 2011. A temperature compensation method for CDOM fluorescence sensors in freshwater. Limnol Oceanogr–Meth. [accessed 2023 Mar 15];9(7):296–301. *https://doi.org/10.4319/lom.2011.9.296*

Watras CJ, Morrison KA, Rubsam JL, Hanson PC, Watras AJ, LaLiberte GD, Milewski P. 2017. A temperature compensation method for chlorophyll and phycocyanin fluorescence sensors in freshwater. Limnol Oceanogr–Meth. [accessed 2023 Mar 15];15(7):642–652. *https://doi.org/10.1002/lom3.10188*

Xu JT, Hood RR, Chao SY. 2005. A simple empirical optical model for simulating light attenuation variability in a partially mixed estuary. Estuaries. [accessed 2023 Mar 15];28(4):572–580. *https://doi.org/10.1007/Bf02696068*

NOTES

Smith S. 2023. Email dated March 13, 2023 to Emily T. Richardson regarding sensor corrections for Xylem (formerly YSI) EXO2 sensors manufactured prior to June 2017.